SUPPLEMENTARY MATERIAL

Ultrasensitive Amplification-free Detection of Circulating miRNA via Droplet-based Processing of SERS tag–miRNA–magnetic Nanoparticle Sandwich Nanocomplex on Paper-based Electrowetting-on-dielectric Platform

Kai-Hao Wang,[#a] Yuan-Yu Chen,[#a] Chih-Hsien Wang,[#a] Keng-Fu Hsu,[b] Lai-Kwan Chau ,[†a] Shau-Chun Wang,[†a] and Yuh-Ling Chen[†c]

[a] Department of Chemistry and Biochemistry and Center for Nano Bio-Detection, National Chung Cheng University, Chia-Yi 62102, Taiwan

[b] Department of Obstetrics and Gynecology, National Cheng Kung University Hospital, Tainan 70101, Taiwan

[c] Institute of Oral Medicine, National Cheng Kung University, Tainan 70101, Taiwan

* Corresponding author.
E-mail: chelkc@ccu.edu.tw (L.-K. Chau); chescw@ccu.edu.tw (S.-C. Wang); yuhling@mail.ncku.edu.tw (Y.-L. Chen)

# These authors contributed equally.

S1. Reagents and materials

Hydrogen tetrachloroaurate (III) trihydrate ($HAuCl_4 \cdot 3H_2O$, 99.99%) and sodium hydroxide were obtained from Showa (Japan). Sodium citrate tribasic dihydrate (99%) and ammonium hydroxide (33%) were purchased from PanReac AppliChem. Safranin O, tetraethyl orthosilicate (TEOS, 99.0%), N-(3-dimethylaminopropyl)-N'-ethylcarbodiimide hydrochloride (EDC, 99.0%), N-hydroxysuccinimide (NHS, 98%), ethanolamine (99.0%), 2-(N-morpholino)ethanesulfonic acid (MES) were acquired from Sigma-Aldrich (USA). (3-Aminopropyl)triethoxysilane (APTES, 98%) was

obtained from Alfa Aesar. (3-Mercaptopropyl)trimethoxysilane (MPTMS) and carboxymethyldextran (CMD) sodium salt (MW = ca. 40000) were procured from Tokyo Chemical Industry (Japan). Ethanol (EtOH, 99%) was obtained from HY Biocare Chemical Enterprise Co. (Chia-Yi, Taiwan). PBS buffer was purchased from Zeus Scientific (Branchburg, NJ). RNase inhibitor (20 U/μL) was procured from Thermo Fisher Scientific. The nucleotide probes containing the locked nucleic acid (LNA™) units and miRNA standards were acquired from GeneWiz (South Plainfield, NJ). Carboxyl-terminated magnetic nanoparticles (MNP) made of Fe_3O_4 with diameter about 6 – 10 nm was obtained from Taiwan Advanced Nanotech Inc. (Taoyuan, Taiwan). Ultrapure water (18.2 MΩ cm) was produced by a Milli-Q water system (Millipore) to prepare all aqueous solutions.

Clear glossy inkjet labels (Color Dance HY-F303) were obtained from Hsin Yun Enterprise Company (Taipei, Taiwan). Silver nanoparticle ink (NBSIJ-MU01) was procured from Mitsubishi Imaging (MPM), Inc. Polytetrafluoroethene (PTFE) thin film of 5 μm was purchased from Polyflon Technology Ltd. (UK). Silicone oil (5 cSt) was acquired from Sigma-Aldrich. The cylindrical magnet containing 4000 Gauss magnetic induction was obtained from U. A. Cultural Enterprises (Taiwan). The diameter and height of this magnet are 2 cm and 1 cm, respectively.

S2. Preparation of LNA probe-functionalized NAEB and MNP

To functionalize NAEB with LNA, NAEBs were coated with CMD with procedures as follows. First, APTES was used to modify the NAEB surface with amine groups by immersing in a 5 mM APTES solution (in 95% ethanol with 0.1% acetic acid) for 2 h. The modified NAEBs was centrifuged for 15 min at 4000×g to remove free APTES, followed by resuspension with MES buffer (50 mM, pH 6.2) containing 10 mg/mL CMD (40kDa) and EDC/NHS (9 mM/18 mM) and shaking for 1 h. Then

CMD-coated NAEBs were coupled with LNA™-1 probe through amine groups. The unreacted carboxylate groups were capped with ethanolamine (0.5 M, pH 8.5). The product NAEB@LNA1 were washed with TE buffer twice prior to storage in a refrigerator at 4 °C.

To functionalize MNP with LNA, one 25 μL aliquot of MNP (10 mg/mL, 2.5×10^{-5} M) was mixed with 975 μL MES buffer and washed twice with MES buffer. The nanoparticles were re-suspended with a MES buffer containing EDC/NHS (9 mM/18 mM) and LNA™-2 probe and shook for 1 h. The unreacted carboxylate groups were capped with ethanolamine (0.5 M, pH 8.5). The product MNP@LNA2 were washed twice with a TE buffer prior to storage in a refrigerator at 4 °C.

The mean sizes of AuNPs and NAEBs were determined by a transmission electron microscope (TEM, JEOL JEM2010). The UV-vis spectra of AuNP solutions and NAEB solutions were obtained by UV-visible spectrometer (UV-Vis-NIR, GBC Cintra 2020). The hydrodynamic diameters of AuNPs in ultrapure water and the zeta potential of NAEBs in ultrapure water before and after coating with CMD were determined by dynamic light scattering (DLS) and zeta potential measurements, respectively, using Zetasizer Nano ZS90 Malvern instrument.

S3. Construction of paper-based electrowetting-on-dielectric (pEWOD) device and conventional magnetic trapping device

We used consumer-grade office printer (Epson's XP-245) to spray conducting liquid of silver nanoparticles from Mitsubishi Imaging on a piece of glossy label paper to fabricate a pre-designed pattern of a series of small fylfot cross-like electrode units as shown in Fig. S1a to produce a disposable pEWOD card. The shape and dimensions of two adjacently interdigitated electrode units are illustrated in Fig. S1b. Each fylfot cross-like unit contained one central square area (0.9 mm × 0.9 mm) with four extended

arms. The ends of two opposite arms were 3.3 mm apart. This area with size 3.3 mm x 3.3 mm was expressly created to fit the lower surface of a pipetted droplet, approximately 50 µL in volume. The interdigitated design enables the loaded droplet to engage with two neighboring units and trigger EWOD movement. The gap between two units was maintained as 0.3 mm, which was less than one-tenth of the electrode unit dimension. This provided the sustained efficiency of EWOD force between the solid and liquid interface.[S1] To place the pEWOD card on the pEWOD device, one piece of PTFE film (7 cm × 4 cm) was fixed on a printed circuit board (PCB) to cover the middle open area and the pins of the PCB, as shown in Fig. S1c. Next, silicon oil was applied on the surface of the PTFE film and then the conducting side of the pEWOD card was placed on the PTFE film. This PTFE film was employed as the dielectric layer of the pEWOD card. Again silicone oil was homogeneously applied on the other side of the PTFE film as a hydrophobic layer. Finally, the leads of the pEWOD electrode pads were aligned to connect with the pins on the PCB. These pins received actuation signals through D-sub connectors.

This assembly of pEWOD card on PCB was stationed on one acrylic housing module, containing a step motor, of which the axis-driven arm can lift one magnet. This motor was also controlled through the micro-controller to position the magnet underneath the pEWOD card. The structure of the pEWOD device is described in Fig. S1c.

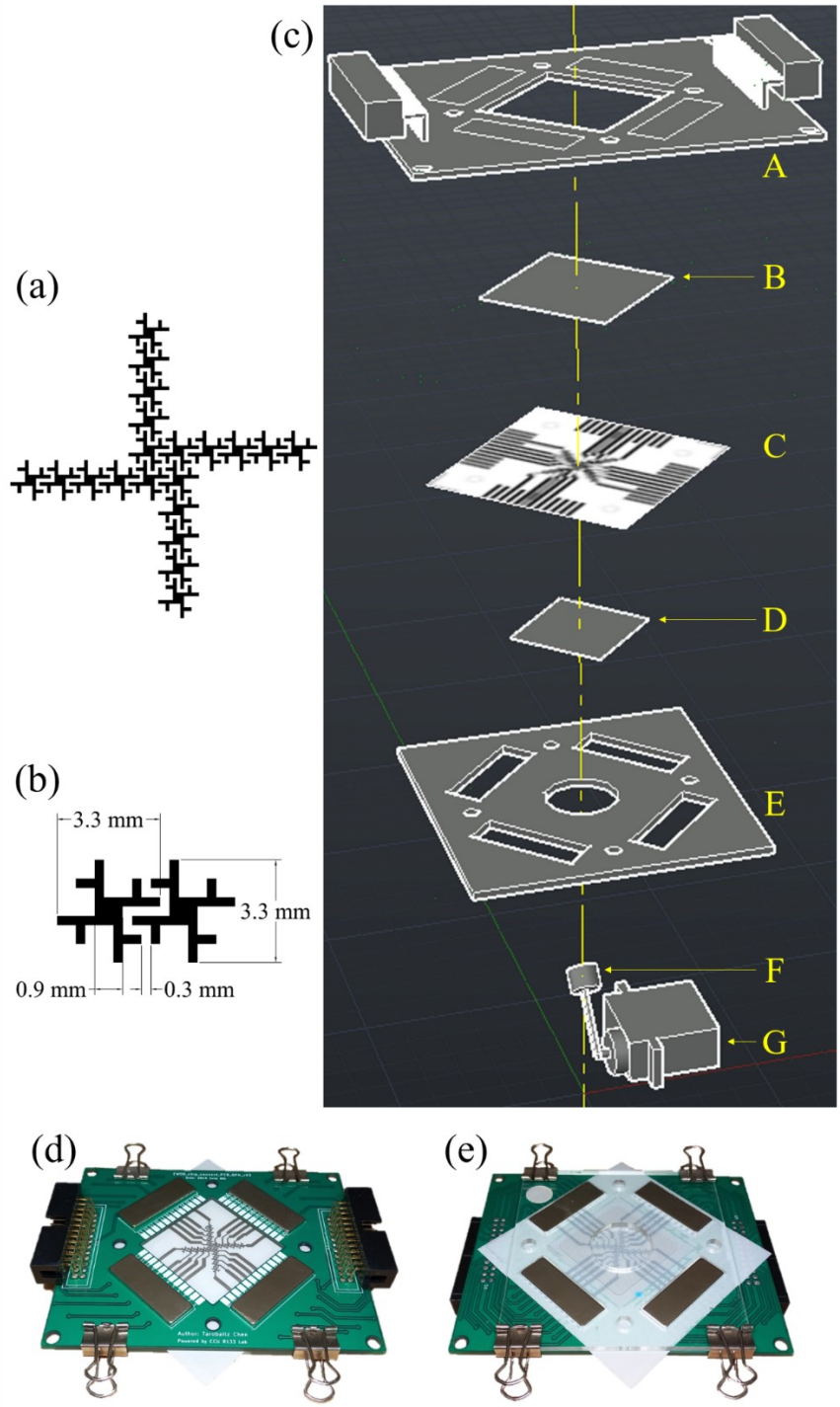

Figure S1. (a) A pre-designed pattern of a series of small fylfot cross-like electrode units to be printed on a glossy label paper. (b) Enlarged view of the shape and dimensions of two adjacently interdigitated electrode units, where each fylfot cross-like unit contains one central square area (0.9 mm x 0.9 mm) with four extended arms as a pEWOD electrode unit. The ends of two opposite arms are 3.3 mm apart. The gap between two units is 0.3 mm. (c) Structure of pEWOD device: A. PCB board; B. PTFE thin film; C. pEWOD card; D. glass cover slip; E: acrylic slide; F: step motor; G. magnet. (d) Top view of pEWOD card on PCB. (e) Bottom view of pEWOD card on

PCB.

In Fig. S2, in-house developed Python codes were used to control an Arduino module, of which the output signals fed into the shift registers on a circuit board. When the relays connected with the register on the same board were triggered in sequence, the hatched high voltage waveforms at each relay were released one-by-one to trigger the pEWOD electrode pads. The loaded droplets were actuated to move. Other micro-controller output signals were used to activate the step motor for positioning one magnet right underneath the pEWOD card to trap MNP-bound miRNA nanocomplex.

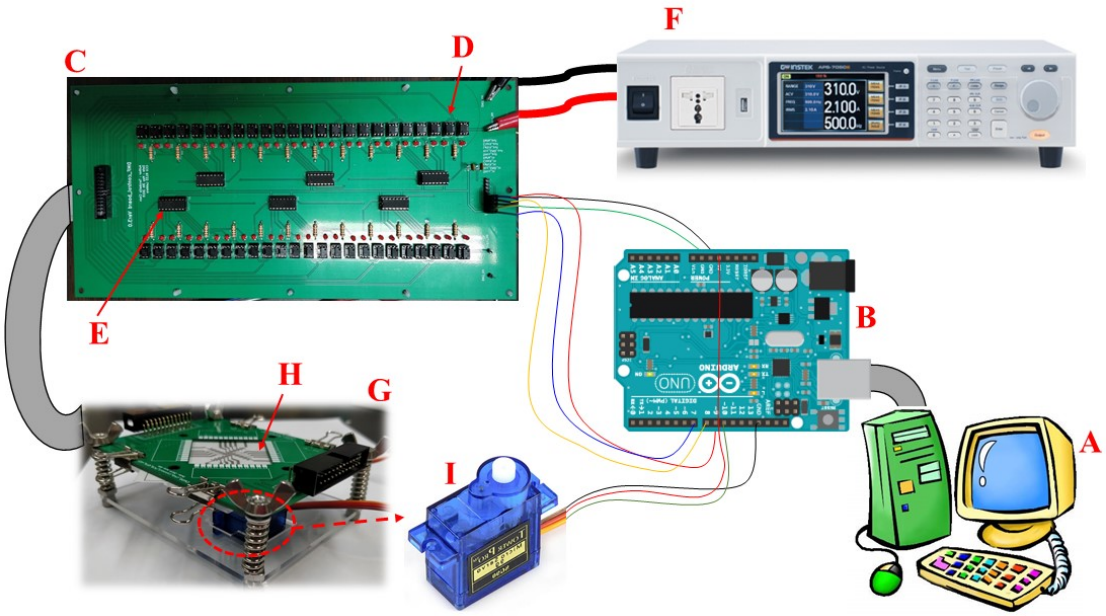

Figure S2. Illustration of pEWOD device containing a disposable pEWOD card: A. Personal computer; B. Arduino micro-controller board; C. Circuit board; D. Registers; E. Relays; F. Power supply; G. pEWOD device; H. pEWOD card; I. Step motor to position magnet.

In line with the apparatus described in our previous publication,[S2] our home-made conventional magnetic trapping device comprised a series of stacked acrylic chips. Each

partially transparent chip had a size of 4.0 × 3.0 cm^2 and a thickness of 0.4 cm. One vertically drilled rectangular slot ran along the center of the device to house the trapping magnet. Another circular hole, with a diameter of 1.1 cm, was drilled vertically. Positioned to extend partially over the edge, this circular hole led to a section of the cylindrical surface being removed, resulting in an open semi-cylindrical slot that functioned as a holder for a collection vial.

S4. Acquisition of Raman spectra

RAMaker from ProTrusTech (Taiwan) was used to acquire the Raman spectra of the reporter molecules in NAEBs of the MNP–miRNA–NAEB nanocomplex. A diode laser from RGB Photonics with 633 nm wavelength and 77 mW focused by a 10X objective lens was used to radiate the samples. The back-scattered light was collected and recorded by Andor Shamrock 193i-B1 spectrograph (UK) with back-illuminated TE-cooled CCD camera (iVac 316; DR-316B-LDC-DD) operated at –40°C. Each spectrum was a sum of 5 exposures of 1 s.

S5. Procedures for qPCR detection

For quantitative PCR (qPCR) detection, total RNA was isolated from 50 µL plasma samples using the miRNeasy Serum/Plasma RNA isolation kit (Qiagen) according to the manufacturer's protocol. Plasma total RNA (14 ng) or synthetic miR-200a-3p (1×10^9 copy/µL) was reverse transcribed into complement DNA (cDNA) using the Mir-X miRNA First-Strand Synthesis kit (Takara Bio USA, Inc.). The reverse transcribed products were then subjected to qPCR analysis using the TB Green® qRT-PCR kit (Takara Bio USA, Inc.). The reverse transcribed product of synthetic miR-200a-3p was serially diluted to a concentration of 1×10^3 to 1×10^9 copy/µL to generate a standard

curve. The primer sequence used are as follows: hsa-mir-200a-3p-F: TAACACTGTCTGGTAACGATGT.

S6. Synthesis and characterization of NAEB and CMD-coated NAEB

For NAEB synthesis, citrate-capped AuNPs were synthesized first as a precursor component. Through the aggregation of AuNPs induced by a bifunctional Raman reporter and the deposition of a silica shell around the nanoaggregate, the NAEBs were formed. The morphology and spectral absorption of the AuNPs and as-synthesized NAEBs were then characterized by using TEM and UV-Vis spectrophotometer, respectively. From the UV-Vis absorption spectrum analysis, the absorption peak of AuNPs is at 520 nm with the average size is 16.0 ± 2.5 nm (Fig. S3). After formation of NAEBs, the major peak at 536 nm was observed in the UV-visible absorption spectra, and the particle size was 108.0 ± 10.8 nm (n = 100) by TEM. Thus, each NAEB particle was composed of 2.9 ± 0.8 AuNPs. The spectral peak red-shift together with a broaden shoulder in the longer wavelength region indicates the formation of NAEBs.

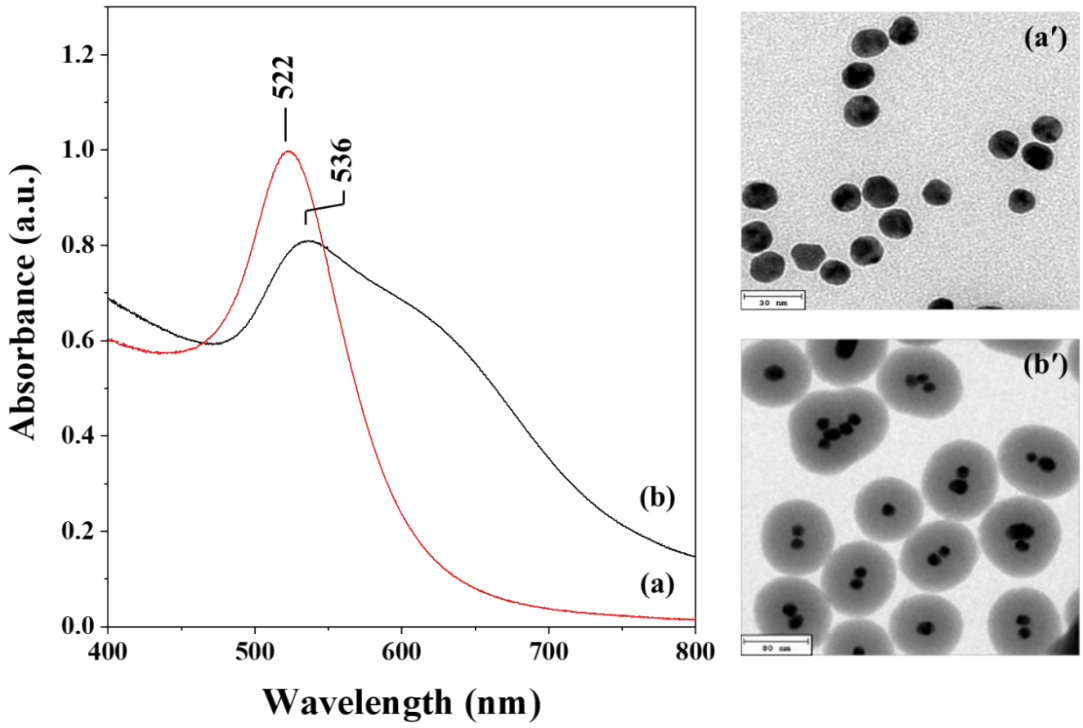

Figure S3. UV-Vis spectra of (a) AuNPs and (b) NAEBs. TEM images of (a′) AuNPs (scale bar = 30 nm) and (b′) NAEBs (scale bar = 80 nm).

S7. Nonspecific binding tests

For these nonspecific binding tests, the procedures followed those in Section 2.3 but in the absence of miRNA. Results as shown in Curve a of Fig. S4 indicates that the nonspecific binding between bare NAEBs and carboxyl-terminated MNPs was negligible, since both the bare NAEBs carry a silica shell and the carboxyl-terminated MNPs are negatively charged at about pH 7. On the other hand, the nonspecific binding between bare NAEBs and MNP@LNA2 was significant (Curve b of Fig. S4), likely due to the adsorption of LNA probe of MNP onto the NAEB's silica surface. Then carboxymethyl dextran (CMD) was coated on NAEBs to reduce the possible nonspecific adsorption of LNA onto the of NAEB surface. As shown in Curve c of Fig. S4, the nonspecific binding between CMD-coated NAEBs and MNP@LNA2 was dramatically reduced.

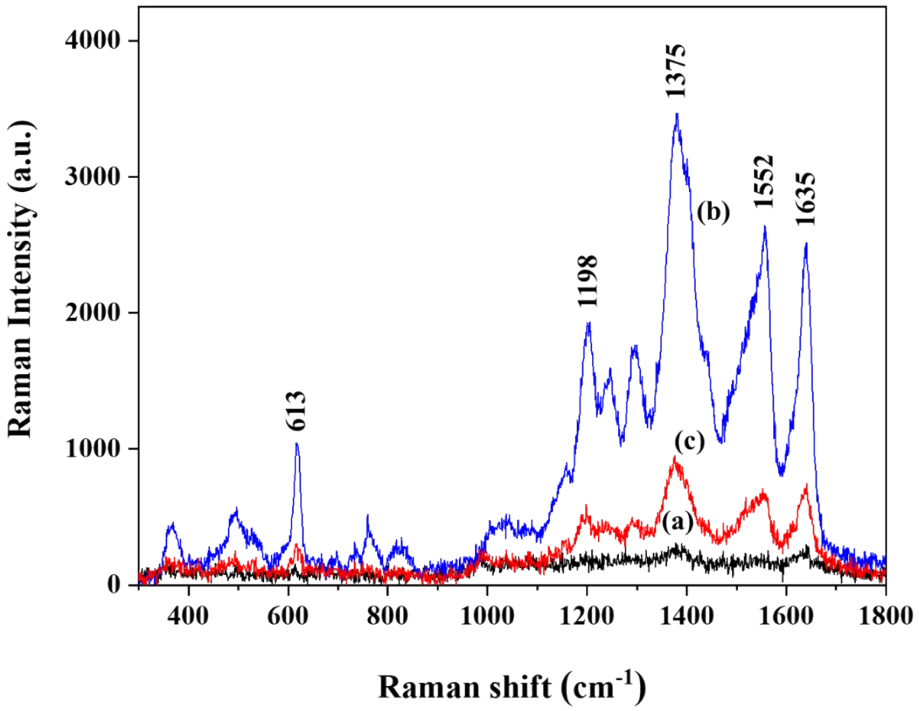

Figure S4. SERS spectra of nonspecific binding tests: (a) bare NAEBs vs MNPs, (b) bare NAEBs vs MNP@LNA2, (c) CMD-coated NAEBs vs MNP@LNA2.

During the CMD coating process, the negatively charged silica surface of bare NAEB first undergoes surface modification by using APTES having a terminal amine group. This modification reduces the negative zeta potential initially, but once the CMD coating is successfully applied, the zeta potential becomes more negative again. These observations are consistent with the zeta potential distribution measurement results shown in Fig. S5.

(a)

Results

		Mean (mV)	Area (%)	St Dev (mV)
Zeta Potential (mV): -31.5	Peak 1:	-31.5	100.0	5.58
Zeta Deviation (mV): 5.58	Peak 2:	0.00	0.0	0.00
Conductivity (mS/cm): 1.51	Peak 3:	0.00	0.0	0.00

Result quality Good

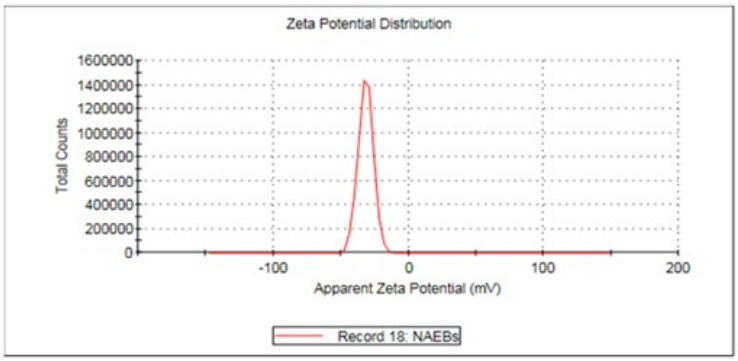

(b)

Results

		Mean (mV)	Area (%)	St Dev (mV)
Zeta Potential (mV): -17.9	Peak 1:	-17.9	100.0	5.21
Zeta Deviation (mV): 5.21	Peak 2:	0.00	0.0	0.00
Conductivity (mS/cm): 1.37	Peak 3:	0.00	0.0	0.00

Result quality Good

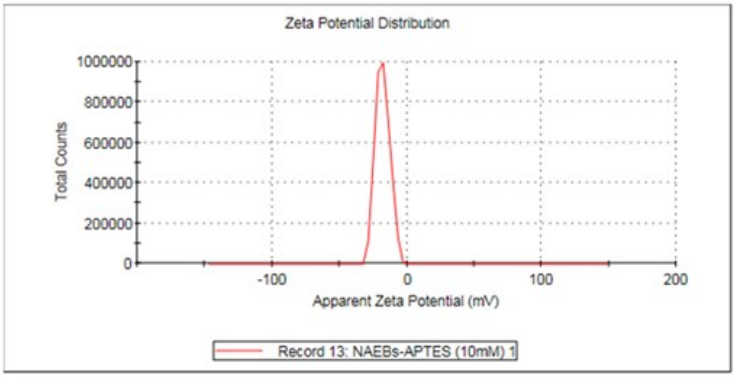

(c)

		Mean (mV)	Area (%)	St Dev (mV)
Zeta Potential (mV): -34.1	Peak 1:	-36.7	91.9	5.45
Zeta Deviation (mV): 10.2	Peak 2:	-4.98	8.1	3.44
Conductivity (mS/cm): 1.38	Peak 3:	0.00	0.0	0.00

Result quality Good

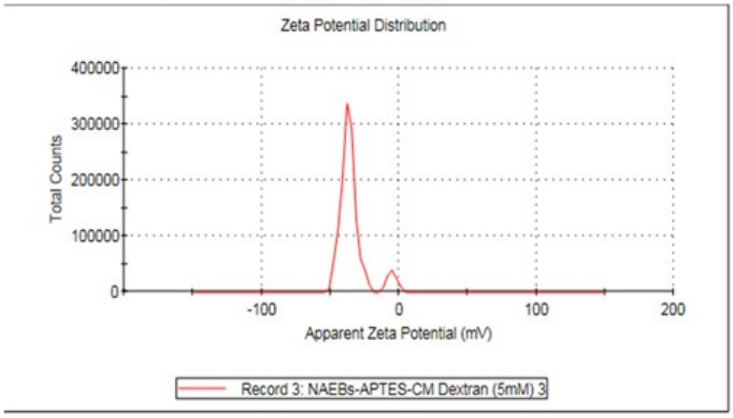

Figure S5. Zeta potential distribution of (a) bare NAEBs, (b) APTES-modified NAEBs, (c) CMD-coated NAEBs.

S8. Processes in magnetic trapping and sample cleanup by pEWOD and conventional magnetic trapping device

The photographic snapshot images of processing MNP–miRNA–NAEB for collection and sample cleanup using pEWOD are shown in Fig. 2. Having loaded the sample droplet of 50 μL containing NAEB–miRNA–MNP nanocomplex on the center of the pEWOD card, we used the step motor to place the magnet underneath the pEWOD card close to the loaded droplet to trap the nanocomplex on the paper card. The supernatant droplet was then driven along one pEWOD electrode to be absorbed by one absorbent pad. Next, this platform moved one smaller droplet (50 μL) containing diethyl pyrocarbonate (DEPC)-treated water and buffer to pick up the remaining sediment on the card center for resuspension. When the ac actuation voltage of 100 Hz was applied to generate capillary wave on the droplet surface, the droplet was vigorously vibrated to resuspend the sediment.[S3] This aforementioned procedures of nanocomplex trapping, supernatant removal, and resuspension of sediment, which typically takes only one minute, were repeated for another three times to thoroughly cleanup the sediment with the nanocomplex formed by miRNA. Finally, the magnetically trapped sediment containing the nanocomplex formed by miRNA was detected using a Raman spectrophotometer.

In comparison, when a 1 mL collection vial containing the NAEB–miRNA–MNP nanocomplexes was positioned in the semi-cylindrical holder slot of the conventional trapping device, magnetic trapping of the nanocomplexes to form solid sediment at the vial wall in proximity to the magnet were gradually observed. After 15 minutes of the trapping process, the supernatant liquid was extracted from the vial using a pipette, and 1 mL of Tris buffer was added to re-suspend the collected solid sediment. This process

of magnetic trapping, supernatant removal, and sediment resuspension took approximately 15 minutes. The process was repeated three times to ensure thorough cleanup of the sediment associated with the miRNA-formed nanocomplexes.

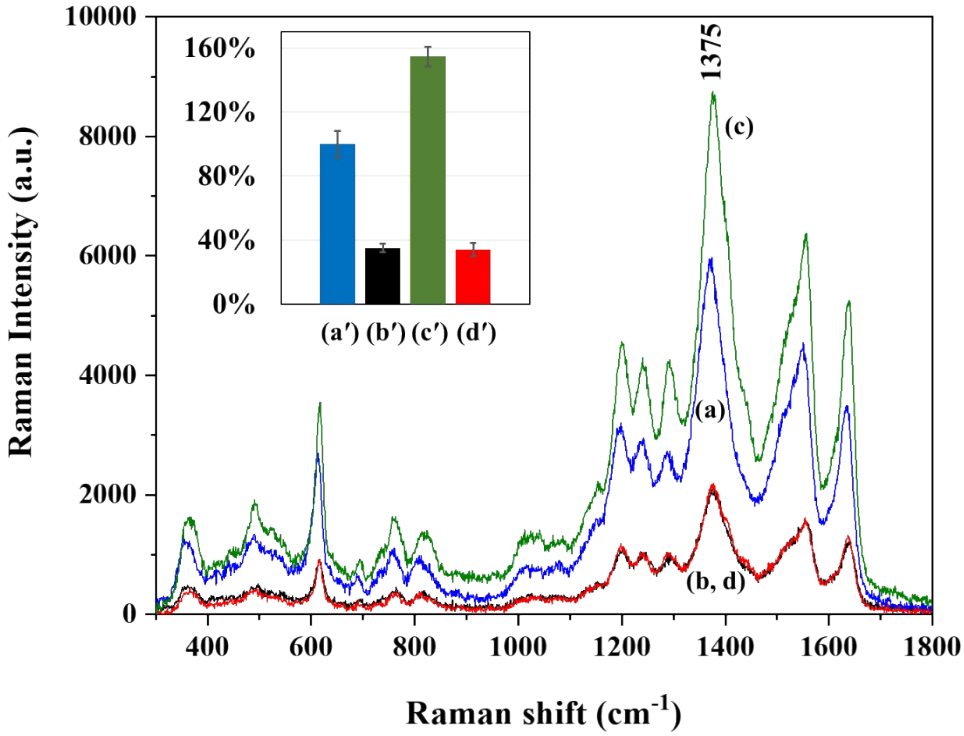

Figure S6. SERS spectra of Safranin O in MNP–miRNA–NAEB obtained by sample pre-treatment methods with (a) conventional magnetic separation rack using 10^{-9} M miRNA-200a-3p sample, (b) conventional magnetic separation rack using blank sample containing no miRNA-200a-3p, (c) pEWOD device using 10^{-9} M miRNA-200a-3p sample, and (d) pEWOD devise using blank sample containing no miRNA-200a-3p. The inset shows the bar graph showing the relative Raman scattering peak intensities at 1375 cm^{-1}.

S9. Detection of miRNA-200a-3p in human plasma samples

The miRNA-200a-3p standards (10^{-9} M) with 5% and 1% healthy human plasma were employed to study the matrix effect. As shown in Fig. S7, the addition of 5% and 1% plasma reduced the Raman intensity of miRNA-200a-3p standard samples by 66% and 24%, respectively. This phenomenon was caused by the presence of the RNase in human plasma resulting in miRNA degradation. Thus, to prevent miRNA degradation,

addition of 10 U RNase inhibitor was determined to be sufficient for miRNA-200a-3p samples (500 μL) containing 1% human plasma. Under these conditions, the Raman intensities of these miRNA-200a-3p standard samples at concentrations of 1 nM, 10 pM, 0.3 pM and 3 fM recovered to 93% to 99% (Table S1). However, the miRNA-200a-3p standard samples containing 5% human plasma could only reach around 80% even in the presence of 50 U RNase inhibitor. The result is possibly attributed to the matrix interference form high concentration of plasma.

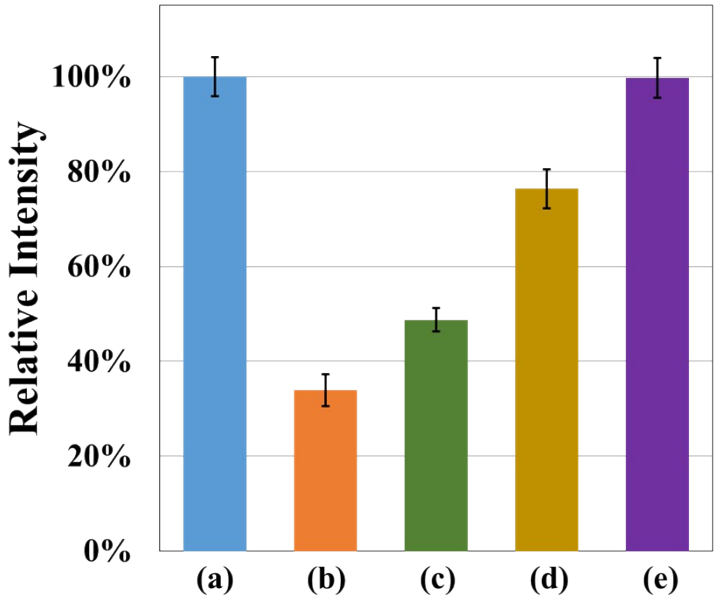

Figure S7. The effects of dilution ratio and RNase inhibitor addition in healthy human plasma samples. Each 500 μL miRNA-200a-3p standard sample under the conditions of (a) no addition of plasma and RNase inhibitor, (b) addition of 5% plasma without RNase inhibitor, (c) addition of 5% plasma and 10 U RNase inhibitor, (d) addition of 1% plasma, (e) addition of 1% plasma and 10 U RNase inhibitor. All miRNA concentrations were 10^{-9} M. Raman scattering intensity (at 1375 cm^{-1}) of sample (a) was designated as 100% relative intensity.

Table S1. Comparison of analytical performance of various amplification-free miRNA biosensors.

Detection technique	miRNA	Linear range	LOD (fM)	Reference
Electrochemical	miRNA-155	10 aM ~ 1.0 nM	0.0057	20
Photoelectrochemical	miRNA-23a-3p	200 fM ~ 2.00 nM	78.9	21
Electrochemiluminescence	miRNA-141	1 fM ~ 10 pM	0.3	22
Field-effect transistor	miRNA21	100 aM ~ 1 nM	0.085	23
Fluorescence	miRNA-155	2.70 fM ~ 0.01 pM	5.2	24
Surface plasmon resonance	miRNA-21		0.010	25
Localized surface plasmon resonance	miRNA-10b		0.083	26
Waveguide interferometric	miRNA-181a		0.023	27
SERS	miRNA-21	4.44 nM ~ 1.48 μM	0.36×10^{-5}	28
SERS	miRNA-21 miRNA-122 miRNA-223	10 fM ~ 100 nM	2.72×10^{-3} 0.24×10^{-3} 2.68×10^{-3}	29
SERS	miRNA-141	120 fM ~ 120 pM	120	30
SERS	miRNA-106a	0.1 pM ~ 100 nM	67.4	31
SERS	miRNA-200a-3p	0.3 fM ~ 1 nM	0.26	This work

Table S2. The results on recovery (N = 3) of Raman intensity of miRNA-200a-3p standard samples containing 1% healthy human plasma and 10 U RNase inhibitor as well as those containing 5% healthy human plasma and 50 U RNase inhibitor at different miRNA-200a-3p concentrations.

Samples (500 μL)	miRNA-200a-3p	Recovery	RSD
1% plasma & 10 U RNase inhibitor	1 nM	99.70%	4.14%
	10 pM	93.22%	6.70%
	0.3 pM	97.35%	5.40%
	3 fM	97.49%	4.30%
5% plasma & 50 U RNase inhibitor	1 nM	77.07%	8.62%
	10 pM	80.28%	3.47%

	0.3 pM	77.40%	5.04%
	3 fM	80.98%	4.45%

Table S3. The measured Raman scattering intensities and CT values and their respective determined miRNA-200a-3p concentrations in 10 real samples. The last column represents the ratio of determined concentration by SERS to that by qPCR.

Method	SERS		qPCR		SERS/qPCR
Sample	Intensity (a.u.)	concentration (M)	CT value	concentration (M)	ratio
N1	2977	1.23E-13	34.21	3.14E-14	3.9
N2	3557	4.72E-13	33.62	4.81E-14	9.8
P3	4408	3.43E-12	30.35	9.00E-13	3.8
P4	2606	5.17E-14	35.02	2.71E-14	1.9
P5	2872	9.61E-14	34.22	2.07E-14	4.6
P6	3807	8.45E-13	33.03	1.91E-13	4.4
P8	3610	5.35E-13	33.62	8.98E-14	6.0
P11	3292	2.55E-13	33.91	7.09E-14	3.6
P13	4080	1.60E-12	32.36	5.12E-13	3.1
P15	2096	1.58E-14	35.47	1.15E-14	1.4

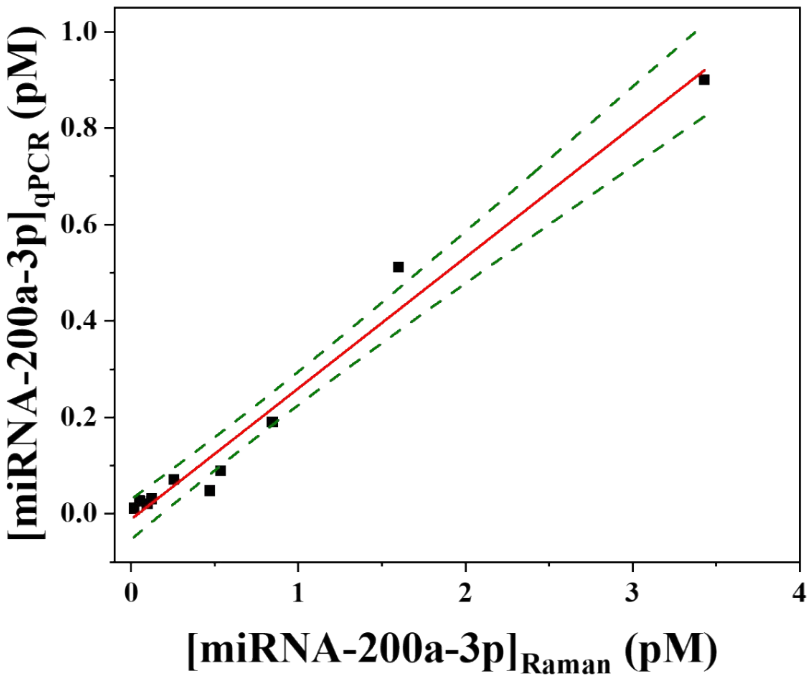

Figure S8. The concentration correlation curve between the results by qPCR and Raman measurement of 10 clinical samples in Table S2. The dash green lines surrounding the best-fit line exhibits the 95% confidence interval for prediction with the regression model.

References:

S1. U.-C. Yi and C.-J. Kim, *Micromech. Microeng.*, **2006**, *16*, 2053-2059.
S2. W. Y. Chen, C. H. Wang, K. H. Wang, Y. L. Chen, L. K. Chau and S. C. Wang, *Biomicrofluidics*, 2020, **14**, 014102.
S3. Y.-Y. Chen, I. J. Ting and S.-C. Wang, *J. Taiwan Inst. Chem. Eng.*, 2021, **126**, 23-28.